超音波マイクロトランスデューサ配列を応用したウェアラブルな閉ループ型経頭蓋脳刺激システムの構築

Construction of a Wearable Closed-loop Transcranial Brain Stimulation System Using an Ultrasonic Microtransducer Array

M22助自50

代表研究者　舘野　高　北海道大学　大学院情報科学研究院　教授
Takashi Tateno　*Professor, Faculty of Information Science and Technology, Hokkaido University*

Neuromodulation is considered a promising tool for treating brain diseases. However, conventional methods are fraught by the attenuation of electromagnetic wave intensity with distance, thereby posing a challenge to its use for the noninvasive induction of transcranial neural responses in deep brain regions. Recently, transcranial ultrasound stimulation has garnered attention because of its low invasiveness and improved spatial resolution. In addition, a mechanical contribution to neural impulse generation could be a physical basis for ultrasound-driven neuromodulation. However, the underlying mechanisms at the cellular level remain unclear. To elucidate the cellular mechanisms, an in vitro experimental system is advantageous as it allows for precise control of the neuronal extracellular microenvironement. However, conventional ultrasound transducers have limited applicability for brain stimulation because of their large size, which prevents the local stimulation of neurons. In particular, the conventional in vitro system has less accuracy in the stimulated area because of the neural activation in relatively wider brain areas. In this study, we have developed a new micro-electro-mechanical systems-based piezoelectric micromachined ultrasound transducer (PMUT) for precise in vitro brain slice stimulation. Numerical simulations were conducted to investigate the correlations between diaphragm dimensions and resonant frequencies. Guided by the numerical findings, we proceeded to design and microfabricate a PMUT featuring four identical circular diaphragms, incorporating eight square recording electrodes. We evaluated the physical properties of the PMUT devices, and finally, we conducted in vitro ultrasound stimulation experiments to evaluate its applicability for neuromodulation. Notably, we found that the PMUT could activate cells. In addition, our PMUT successfully detected neural activities with the incorporated electrodes. Thus, the PMUT device can be used both for stimulation and recording. We aim to apply this device for closed-loop ultrasound stimulation and small and wearable devices in our future studies.

研究目的

近年、神経疾患等の症状を改善する目的で、脳刺激法の研究開発が進められている。従来の電磁気的な脳刺激法では、脳深部を高空間分解能で局所刺激する場合に、刺激装置の先端部を脳内に直接刺入するか、もしくは、刺激用インタフェースを標的部位に接近させる必要があり、侵襲性が非常に高かった。また、脳内に刺激部を留置しない、非侵襲的な方法である経頭蓋刺激法では、刺激位置直下の脳表とその近隣の脳領域のみの標的部位に対象が限られて神経活動が誘発される欠点があった。本課題では、これら欠点を根本的に解決するため、中枢神経系の経頭蓋脳刺激法として、脳深部まで刺激効果が到達可能な低強度の集束超音波を開発することを目的とした。低強度の集束超音波は、破壊を伴わずに脳活動を誘発する非侵襲的な方法として有望であるにも関わらず、現時点では装置開発が未開拓な分野であり、その開発が特に臨床的に期待されている。本課題では、神経疾患の症状制御を目的として、神経活動シグナル（脳波）を持続的に経頭蓋でモニターしながら、閉ループ型の制御によって介入が必要な時のみに脳深部に頭蓋骨を介して低強度集束超音波の抑制性刺激を印加するシステムの基盤技術を開発した。具体的には、集積化を目指して、微細加工技術を用いて記録用電極とマイクロサイズのトランスデューサを併設したデバイスを開発し、神経組織切片を利用して製作デバイスの特性を評価した。

概　　要

Neuromodulation is considered a promising tool for treating brain diseases. However, conventional methods such as transcranial direct current and magnetic stimulation are fraught by the attenuation of electromagnetic wave intensity with distance, thereby posing a challenge to its use for the noninvasive induction of transcranial neural responses in deep brain regions. Recently, transcranial ultrasound stimulation has garnered attention because of its comparatively low invasiveness and improved spatial resolution.

While neural impulses have conventionally been regarded as electrical signals, it is noteworthy that the suprathreshold depolarization of excitable membranes in neurons is also influenced by mechanical mechanisms in addition to eletrophysiological mechanisms. Hence, a mechanical contribution to neural impulse generation could be a physical basis for ultrasound-driven neuromodulation. However, the underlying mechanisms at the cellular level remain unclear. To elucidate the cellular mechanisms, an in vitro experimental system is advantageous as it allows for precise control of the neuronal extracellular microenvironement. However, conventional ultrasound transducers have limited applicability for brain stimulation because of their large size, often exceeding 10 mm, which prevents the local stimulation of neurons (i.e., within the range of tens to a few hundred microns). In particular, the conventional in vitro system has less accuracy in the stimulated area because of the neural activation in relatively wider brain areas.

Several previous studies introduced a piezoelectric micromachined ultrasound transducer (PMUT) and validated its efficacy in elucidating the cellular mechanisms of neuromodulation through experiments conducted on dissociated cultured neurons in vitro. However, in their experiments, the neural networks consisted

of random connections, as neurons within the source neural tissue lost their original network connections during the dissociation process for in vitro culture. Acute brain slices are therefore more appropriate in vitro preparations for understanding the biological mechanisms of ultrasound-mediated modulation of neural activity. In addition, conventional open-loop stimulators have a risk of over-inducing neural activity during protracted use, resulting in artificial responses, while closed-loop stimulation is expected to reduce the adverse effects of excessive stimulation. Furthermore, there are several reports of wearable capacitative micromachined ultrasound transducer (CMUT) devices for small animals. Compared to PMUTs, CMUTs, including microdevices, have limited applicability for in vivo use in animals becase a high bias voltage (e.g., 100 V) is required, in addition to the driving AC voltage, for stimulation.

In this report, we described the development of a new MEMS-based PMUT for precise in vitro brain slice stimulation. Numerical simulations were conducted to investigate the correlations between diaphragm dimensions and resonant frequencies. Guided by the numerical findings, we proceeded to design and microfabricate a PMUT featuring four identical circular diaphragms, each with a radius of 580 μm, and incorporating eight square recording electrodes of 200 μm × 200 μm. To our knowledge, this is the first report of the incorporation of recording electrodes onto a PMUT. We evaluated the physical properties of the PMUT devices, and finally, we conducted in vitro ultrasound stimulation experiments to evaluate its applicability for neuromodulation. Notably, we found that the PMUT could activate cells. In addition, our PMUT successfully detected neural activities with the incorporated electrodes. Thus, the PMUT device can be used both for stimulation and recording. We aim to apply this device for closed-loop ultrasound stimulation in our future studies.

本　文

1. Summary

In this study, we first designed a piezoelectric micromachined ultrasound transducer (PMUT) device structure after computations were performed to identify conditions that would allow for the desired physical properties, including the relationship between the resonant frequency and the size of transducers (circular diaphragms). For closed-loop ultrasound stimulation, we incorporated recording microelectrodes onto the same device as the PMUT. Second, we microfabricated the PMUT devices and measured their physical properties and compared with those initially aimed for. Third, to examine the potential of our fabricated device for neuromodulation, we measured the PMUT-driven cellular responses in acute mouse brain slices. Finally, to assess the applicability of the interface in a closed-loop system, we recorded neural activity in brain slices with microelectrodes fabricated onto the device.

2. Materials and Methods

2.1 System Design

To record neural responses locally from brain slices, we aimed to develop a PMUT device that satisfied two stimulation conditions and a size condition: (i) a resonant frequency of the diaphragm of 500 kHz; (ii) an ultrasound pressure for stimulation greater than 65 kPa; and (iii) a diaphragm radius smaller than 600 μm (Lee et al.,

2019; Oh et al., 2019). Our PMUT device consists of the following five components: a lead zirconate titanate (PZT) film, a silicon (Si) layer, a SiO_2 membrane, top and bottom Pt/Ti electrodes, and a Si supporting layer (figure 1(a), (b)). To operate as a transducer, a thin film of a piezoelectric material was used to convert electric (voltage) signals into ultrasound pressure changes. To obtain a thin diaphragm functioning as a vibrating plate, circular openings were strategically designed from the rear side of the supportive Si substrate (figure 1(a)).

Before fabricating the device, we numerically simulated the vibrations of diaphragms in the PMUT using general-purpose physics simulation software (COMSOL Multiphysics, Ver. 5.5, COMSOL AB, Sweden). Using the finite-element method (FEM) in this simulation software, we calculated the resonant frequency (500 kHz) and determined the sizes of the PMUT. In particular, the objective of the numerical computation was to ascertain the suitable radius (r) of the diaphragm, along with the thicknesses of the piezoelectric material and Si-supporting layers, ensuring resonance of the diaphragm in response to a 500 kHz input frequency. All parameters, including the thicknesses of the layers, are summarized in Table 1. To confirm the results of the numerical calculation, an analytical calculation was performed and compared it with the numerical results, as previously reported (Wah, 1962; Muralt et al., 2005; Furukawa and Tateno, 2022).

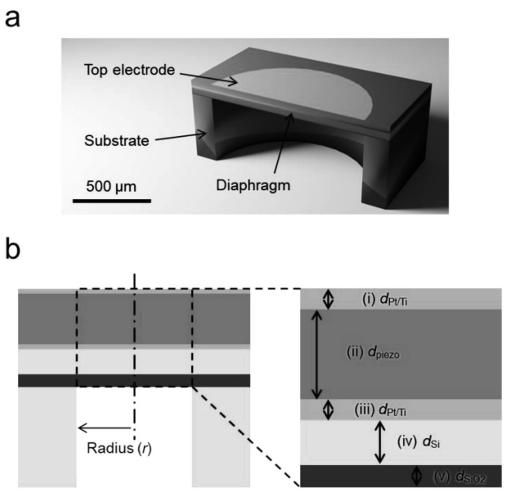

Figure 1 Schematics of the PMUT. (a) Illustration of a diaphragm of the device. (b) Cross-section of the PMUT, which consists of four components—a piezoelectric material (PZT), Si, SiO_2, and Pt/Ti.

2.2. Microfabrication Processes

To achieve precisely localized brain slice stimulation, the PMUT was engineered with an array comprising four diaphragms, offering high spatial resolution (figure 2). The PMUT had the dimensions of a 15 mm^2 square. Microelectrodes (200 μm × 200 μm) were designed on the substrate to simultaneously record the electrical activity of the brain slice (figure 2(a,b)).

The fabrication process was based on a previous report on the standard microelectromechanical system (MEMS) technology (Kuwano et al., 2020). The initial substrate was a silicon-on-insulator (SOI) wafer consisting of the following three layers: a device layer (Si, 15 μm), an insulating membrane (SiO_2, 1 μm), and a handle layer (Si, 500 μm).

Our microfabrication process was illustrated in figure 3. After the process, the fabricated PMUT

Table 1 Material parameters used in the numerical calculation.

Material	Thickness in μm	Young's modulus in GPa	Density in kg/m^3	Poisson's ratio
PZT	d_{Piezo}	63	7500	0.34
Si	d_{Si}	170	2329	0.28
SiO_2	d_{SiO2}	70	2200	0.17
Pt	d_{Pt}	168	2145	0.38

device was packaged with the printed circuit board.

2.3. Physical Properties

To assess the characteristics of the produced PMUTs, we conducted measurements of the resonant frequencies of the diaphragms. A custom-made PCB was affixed with a cylindrical acrylic chamber, having an internal diameter of 30 mm, onto the substrate (figure 4(a)). Initially, each diaphragm within the PMUT was actuated using a sinusoidal voltage signal of 10 V amplitude, and amplified through a radio-frequency amplifier with a 10-fold voltage gain. The frequency range was 260–900 kHz. The acoustic pressure generated immediately above the diaphragm within the chamber was assessed using a calibrated needle hydrophone. During the measurement, the frequency (among the applied frequency range of 260–900 kHz) eliciting the highest peak response was designated the resonant frequency of the applied voltage signal. Each measurement consisted of five trials at the same conditions.

Furthermore, we assessed the electrical characteristics of microelectrodes using electrochemical impedance spectroscopy (EIS). To characterize the electrochemical properties of the microelectrodes on the PMUT device, we used a potentiostat with a built-in frequency

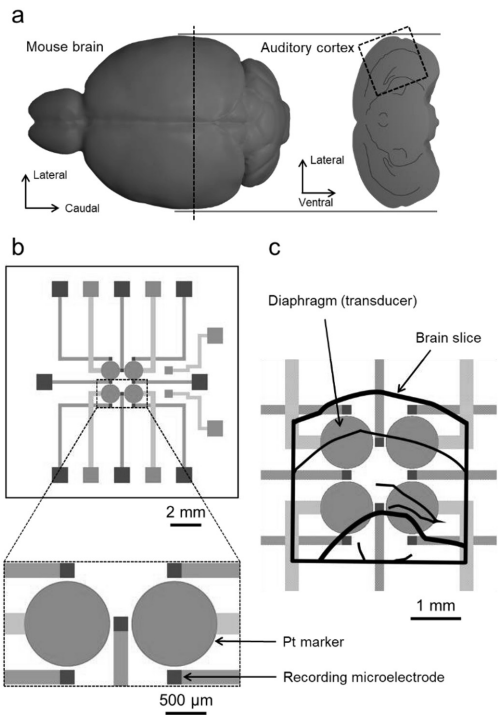

Figure 2 Design of the PMUT and recording electrodes with readout pads. (a) mouse brain and a slice (b) Overall patterns of the PMUT design (top view; upper panel) and the enlarged view of the center part (lower panel). (c) Diaphragms and microelectrodes illustrated with a brain slice.

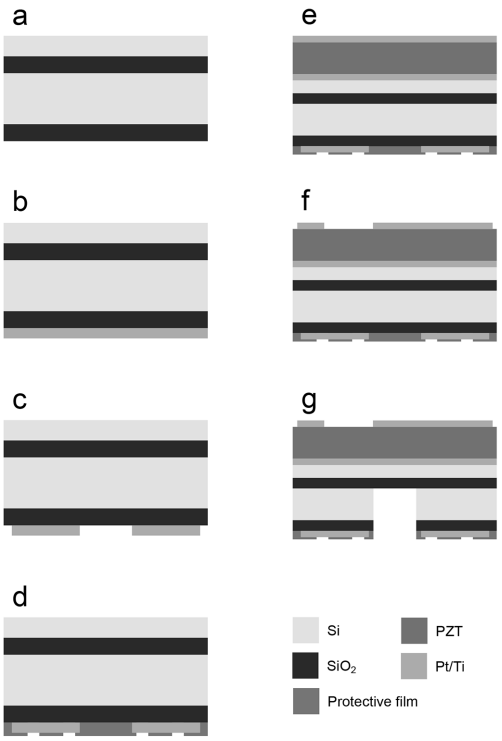

Figure 3 Microfabrication processes used to construct the PMUT. The different colors represent the different materials— Si, PZT, SiO_2, Pt/Ti, protective film, and epoxy resin E205. The thickness of each material indicated in the figure does not reflect its actual size.

analyzer. Microelectrodes were tested using a three-electrode test apparatus. A standard calomel electrode and a platinum wire of 0.2-mm diameter served as the reference electrode and counter electrode, respectively. Forty sinusoidal voltage waves with an amplitude of 25 mV were applied to each microelectrode (Takahashi et al., 2019).

2.4. Preparation of Brain Slices

In the present study, we used four C57BL/6J mice. Each mouse was deeply anesthetized with isoflurane and decapitated, and the brain was quickly removed and placed into ice-cold artificial cerebral spinal fluid (ACSF) solution. During the sectioning of brain slices containing the auditory cortex, the measurement of the distance along the rostral/caudal axis from the bregma was performed for each coronal section according to the following protocol. For visual representations of mouse brain coronal sections, we employed a digitized atlas (Franklin and Paxinos, 2007). Coronal slices, 400 μm thick, encompassing the auditory cortex, were obtained using a tissue slicer in chilled ACSF. All slices were left in a chamber for 2 h (Furukawa et al., 2022).

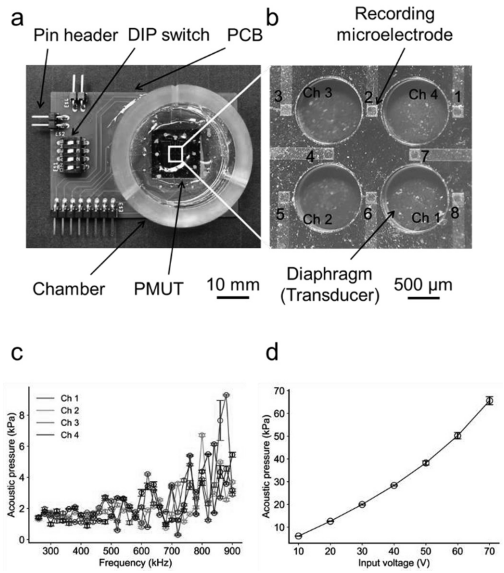

Figure 4 Images of the microfabricated PMUT on a PCB substrate and the physical properties of diaphragms. (a) The packaged substrate with the PMUT device. (b) The front side of the PMUT with four diaphragms (channels [chs] 1 to 4) and eight electrodes (1 to 8). Numbers represent chs of the electrodes to specify each of them. (c) Measured acoustic pressure of diaphragms as a function of frequency in response to a sinusoidal voltage input to them. (d) Representative resonant acoustic pressures with different input voltages at the driving frequency of 880 kHz, which is also equivalent to the resonant frequency.

2.5. Calcium Imaging

In this study, PMUT-driven intracellular activity was observed using chemical fluoresent Ca^{2+} indicators. Our selection criteria for the indicators were (i) a relatively high Ca^{2+} affinity (dissociation constant (Kd) < 400 nM) and (ii) spectral properties in imaging: i.e., single-wavelength imaging. Thus, we selected the popular single-wavelength indicator Fluo-4 AM, whose Kd is around 345 nM (Paredes et al., 2008).

2.6. Neural Activation of Cells in a Brain Slice

Ultrasound stimulation (US) using the PMUT was directly applied to cells in a brain slice. In the absence of stimulation, we first monitored the baseline changes in Ca^{2+} transients for 1 s as the Pre-US. Successively, we applied ultrasound stimulation (880 kHz continuous wave) for 1 s, and imaged the Ca^{2+} transients, followed by monitoring of Ca^{2+} transients during the recovery period for 1 s (total of 3 s per trial). We also monitored Ca^{2+} signals evoked by sham stimulation, i.e., stimulation generated by the PMUT with 0 V input voltage. During the recordings, slices were placed

on PMUT substrates and covered with nylon mesh and a stainless slice anchor at room temperature (23.6 ± 0.8 °C).

2. 7. Microelectrodes for Recording Activity in a Brain Slice

For local field potential (LFP) recordings, we recorded spontaneous and seizure-like neural activities induced by standard (normal) and magnesium (Mg^{2+})-free ACSF, respectively (Anderson et al., 1986). In each slice, spontaneous activities in normal ACSF were firstly recorded as a control for 5 min. Subsequently, we perfused Mg^{2+}-free ACSF for 25 min and performed the recording for 5 min. The signals were recorded with a sampling rate of 20 kHz and subjected to filtering within a frequency range of 1 Hz to 10 kHz. To compare the temporal properties in control and Mg^{2+}-free conditions, we analyzed the power spectra of extracellular recording signals.

3. Results

3.1. Microfabrication of the PMUT

On the basis of the results of computational simulation of the PMUT model having a resonance frequency of 540 kHz, a diaphragm with a radius of 580 μm, a PZT layer thickness of 100 μm, and a Si layer thickness of 15 μm was selected. The numerically calculated resonant frequency (i.e., f_c = 540 kHz) was not the same as the originally designed frequency (500 kHz). However, we decided to use this f_c. Ultrasound stimulation has an effective range of frequencies, and 540 kHz is within this range (Li et al., 2023). Subsequently, the PMUT device comprising four diaphragms and eight microelectrodes was fabricated using microfabrication techniques. Then, the PMUT device was packaged on a PCB substrate. A PMUT is illustrated in figure 4(a).

3.2. Physical Characteristics of the Fabricated PMUT

To assess the response of the manufactured PMUT, we initially conducted measurements of the acoustic pressure generated by individual diaphragms. The PMUT was driven by sinusoidal voltage signals of varying frequencies, but of constant voltage (V_{in} = 10 V) (figure 4(c)). A typical example of the frequency response for four diaphragms (channels 1 to 4) is illustrated in figure 4(c) for an input frequency of 260–900 kHz. For the pressure measurements, the first peak acoustic pressure was always acquired at a higher frequency (f_{peak}) than the resonant frequency (i.e., f_r = 540 kHz) estimated in the simulation. For one PMUT device, for example, the error ($|f_{peak} - f_r|$) rate of the four diaphragms was 55 ± 3% (mean ± standard error of the mean (SEM); figure 4(c)). Overall, the error rate of the six diaphragms in the examined PMUT devices was 40 ± 10%.

Subsequently, to examine the input voltage-dependency of the PMUT, we conducted measurements of the acoustic pressure generated by individual diaphragms. The PMUT was actuated using sinusoidal voltage signals at a consistent frequency (AC amplitude of 10–70 V; figure 4(d)). When the input voltage amplitude was increased, the output acoustic pressure at the measured resonant frequency (f_{peak} monotonically increased (figure 4(d)). On the basis of these results, we applied an acoustic pressure of 65.6 ± 1.8 kPa (for an input voltage of 70 V) of ultrasound stimulation to brain slices *in vitro*.

3.3. Calcium Imaging

To examine whether our PMUT could activate cells, the fluoresence Ca^{2+} indicator (Fluo-4 AM) was loaded onto seven brain slices. First, a typical fluorescent image of a typical brain slice is shown in figure 5(a). In the fluorescent image, a cell body is indicated by an arrow. Ultrasound stimulation was generated for a 1-s period by the PMUT driven by the 70 V sinusoidal signal at an oscillatory frequency of 880 kHz. After the stimulation onset, the florescence signal of the cell increased gradually and was sustained for at least 1 s, even after the stimulation was turned off (figure 5(b)).

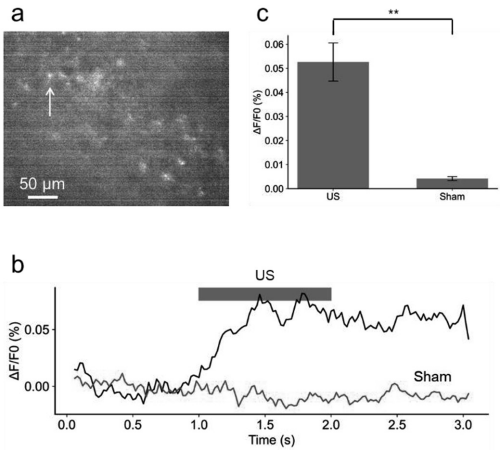

Figure 5 Fluorescence Ca^{2+} imaging of brain slices driven by the fabricated PMUT and response characteristics. (a) Fluorescent image of cells in a brain slice stained with Fluo-4 AM dye. Small areas appearing bright in the image represent cell bodies. A typical cell is indicated by an arrow. (b) Representative fluorescence transients of cell responses evoked by ultrasound stimulation (frequency, 880 kHz; acoustic pressure, 65.6 ± 1.8 kPa; duration, 1 s) by the PMUT. The red line shows the transient under the sham condition (acoustic pressure, 0 kPa). (c) Response average (maximum) amplitude with two conditions: (i) ultrasound stimulation (65.6 ± 1.8 kPa) and (ii) sham stimulation (0 kPa). Data are indicated as the mean ± SEM (n = 5 in two slices). Mann–Whitney U-test was used to analyze the difference. **$p < 0.01$.

As a control experiment (sham condition), when ultrasound stimulation was applied for the same duration with a 0 V sinusoidal input signal, the fluorescence signal did not increase (figure 5(b)).

To test the difference between two conditions (70 V vs. 0 V), we statistically analyzed the response amplitudes, which were defined as the maximum intensity in the stimulus period. The response amplitude under ultrasound stimulation was significantly larger than that under sham stimulation ($p = 0.008$; $n = 5$, two slices; figure 5(c)). This result indicates that our device has the potential to activate cells in brain slices, because the calcium signals of cells in the brain slice were synchronized with the membrane voltage changes.

3.4. Recording of LFPs in a Brain Slice

The PMTU device was incorporated with recording microelectrodes (200 μm × 200 μm) to record electrical activity from brain slices. The impedance of the microelectrodes was 23.4 ± 3.7 kΩ (at 1 kHz; eight electrodes). Thus, the fabricated microelectrodes with low impedance would be useful for recording LFPs from brain slices.

In addition to constructing a closed-loop feedback system for the PMUT device, we were interested in examining the device's ability to detect spontanous neural activity during the sleep-wake cycle, as well as short-term memory and other brain functions. The representative LFPs in spontanous activity acquired on channel 7 under normal conditions are, as an example, shown in the top panel of figure 6(a),(b). The spontaneous activity in the normal ACSF condition showed fast negative peaks. The negative peaks of repid changes in LFPs occurred randomly during recording periods, and the inter-event intervals

were 15.5 ± 1.1 s for the seven channels analyzed for examined slices.

In the brain, extracellular (interstitial) Mg^{2+} concentration ($[Mg^{2+}]_o$) is maintained at 0.7–1.3 mM (Sun et al., 2009). Many studies of $[Mg^{2+}]_o$ in cortical brain areas focused on voltage-dependent blockade of the NMDA receptor, restricting its opening to more depolarized potentials in cell membraines. Thus, to test our device under low $[Mg^{2+}]_o$ conditions, we perfused the brain slices with 0 mM $[Mg^{2+}]_o$ ACSF solution. Eliminating Mg^{2+} (0 mM $[Mg^{2+}]_o$) induced seizure-like activity, with more events with small positive peaks than those with negative peaks across the baseline voltage (figure 6(a),(b)).

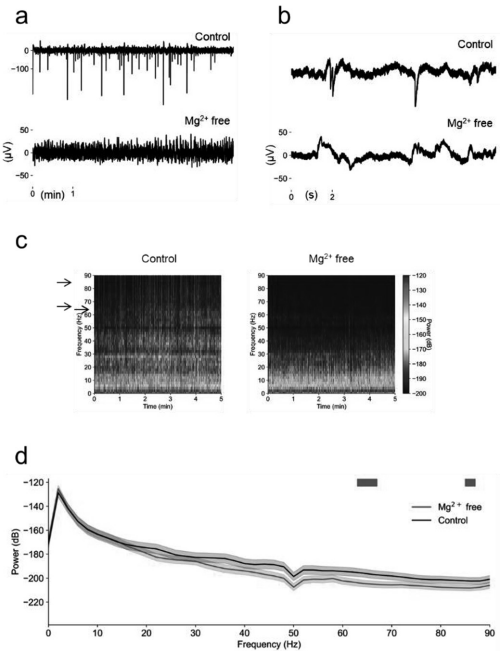

Figure 6 Spontaneous activity recording of brain slices using microfabricated electrodes incorporated into the PMUT. (a) Local field potential (LFP) recordings during spontaneous activity in normal (1.3 mM of extracellular Mg^{2+} concentration) ACSF and in Mg^{2+}-free (0 mM) ACSF. Three typical LFP waveforms are illustrated for (i) the control condition (top trace) and (ii) immediately after the switch to Mg^{2+}-free condition (bottom trace). (b) Expanded views of spontaneous activity events in panel (a). The time intervals of the original traces are indicated by arrows in panel (a). (c) Time–frequency analysis of the three LFP waveforms (duration, 5 min) illustrated in panel (a). (d) Power spectra of LFP waveforms. The blue bars indicate significant differences among the frequencies (64, 66 and 86 Hz; p = 0.037, 0.043 and 0.045, respectively).

Furthermore, we compared the power spectra of the LFP transients for all eight channels in all three slices (figure 6(c)). We found that both early and delayed switch to Mg^{2+}-free conditions produced a tendency towards a reduction in high-frequency power (figure 6(c)). In addition, as shown in figure 6(d), we found that high-frequency powers (64, 66 and 86 Hz) in the Mg^{2+}-free ACSF were significantly smaller than those in normal ACSF (n = 24, p = 0.037, 0.043, and 0.045, respectively).

4. Discussion

The measured resonant frequency (i.e., f_{peak} = 835 ± 17 kHz) was not the same as the calculated resonant frequency (540 kHz). One of the possible reasons for the shift to higher frequency is the difference in module selection in the computational simulation. In this study, the mechanics module was only used in the design. However, the elevation of the resonant frequency of the vibration could be seen by adding the electrostatics module to the mechanics module. Therefore, the use of a hybrid module is required in future work.

Although among the individual diaphragms of one PMUT device, the frequency–response characteristics were not identical, the variance of the error rate was small (SEM = 3%). In total, for the two PMUT devices, the error rate of six diaphragms was 40 ± 10%, which was relatively larger than that for similar PMUT devices reported

in previous studies (14–40%) (Cheng et al., 2019; Dangi et al., 2020). For this reason, there could be a discrepancy between the fabricated and designed layer thicknesses of the individual diaphragms. To test this hypothesis, we will use scanning electron microscopy to measure the thicknesses of the individual layers in future studies.

We observed significant calcium influx with ultrasound stimulation by the PMUT. This suggests that our fabricated PMUT can be used for neuromodulation in brain slices. Thus, our microdevice can be used to modulate the activity of cells in cortical slices, and should therefore be useful for elucidating the mechanisms of ultrasound-driven activities in the cortex.

In this study, we applied fluorescent Ca^{2+} indicators to brain slices, which included not only neurons, but also glial cells. Therefore, the fluoresence signals observed in the experiments would be a maixture of neuronal Ca^{2+} transients combined with glial Ca^{2+} waves. This would suggest that it might be diffcult to distinguish these two types of signals in brain slices. However, in this study, we observed mainly two kinds of cellular responses: (i) slow and strong responses over a long duration (figure 5(b)) and (ii) rapid responses synchronized with the stimulation onset (data not shown). In general, glial cells usually exhibit slow transients in intracellular Ca^{2+} signals, whereas neuronal responses are rapid, but decrease within a window of hundreds of milliseconds (Ikegaya et al., 2005). Thus, these temporal differences in Ca^{2+} signals might be derived from differences in cell types in a brain slice.

Because our PMUT combined with microelectrodes could also detect spectral changes in electical activities in brain slices, a feedback system consisting of a real-time detector of abnormal activities could be implemented in future applications. Although we presented a PMUT for *in vitro* ultrasound stimulation, this miniaturized transducer with recording electrodes would be a useful tool for *in vivo* experiments as well. Although there are several reports of closed-loop ultrasound stimulation systems (Dong et al., 2023; Xie et al., 2022), their stimulation and recording modules were completely separated. In comparison, our packaged interface is amenable to a compact closed-loop system. We will apply our new packaged system for chronic closed-loop stimulation and monitoring in future studies.

参考文献

［1］ W. W. Anderson et al., Brain Res, vol. 398, no. 1, pp. 215-219, Nov. 1986.

［2］ C. Y. Cheng et al., IEEE Trans Ultrason Ferroelectr Freq Control, vol. 66, no. 10, pp. 1605-1615, 2019.

［3］ A. Dangi et al., IEEE Trans Ultrason Ferroelectr Freq Control, vol. 67, no. 4, pp. 801-809, 2020.

［4］ S. Dong, et al., Cerebral Cortex, May 2023, doi: 10.1093/CERCOR/BHAD174.

［5］ K. Franklin and G. Paxinos, The Mouse Brain in Stereotaxic Coordinates. 2007.

［6］ R. Furukawa and T. Tateno, in In Proceedings of International Joint Conference on Biomedical Engineering Systems and Technologies (BIOSTEC 2022), 2022, pp. 196-203.

［7］ R. Furukawa, H. Kaneta, and T. Tateno, Front Neurosci, vol. 16, no. February, pp. 1-19, 2022.

［8］ T. Kuwano, et al., IEEJ Transactions on Electrical and Electronic Engineering, vol. 15, no. 12, pp. 1816-1823, 2020.

［9］ Y. Ikegaya, et al., Neurosci Res, vol. 52, no. 2, pp. 132-138, 2005.

［10］ J. Lee et al., Microsyst Nanoeng, vol. 5, no. 1, 2019.

［11］ Z. Li, et al., Front Psychiatry, vol. 14, p. 646, Apr. 2023.

［12］ P. Muralt et al., IEEE Trans Ultrason Ferroelectr

Freq Control, vol. 52, no. 12, pp. 2276-2288, 2005.
［13］ S. J. Oh et al., Current Biology, vol. 29, no. 20, pp. 3386-3401.e8, 2019.
［14］ L. Sun, et al., Magnes Res, vol. 22, no. 4, pp. 266-272, Dec. 2009.
［15］ R. M. Paredes et al., Methods, vol. 46, no. 3, pp. 143-151, Nov. 2008.
［16］ S. Takahashi, et al., IEEJ Transactions on Electrical and Electronic Engineering, vol. 14, no. 2, pp. 303-311, 2019.
［17］ T. Wah, J Acoust Soc Am, vol. 34, no. 3, pp. 275-281, 1962.
［18］ Z. Xie, et al., Front Neurosci, vol. 16, no. September, pp. 1-12, Sep. 2022.

今後の研究の見通し

本研究課題では、超音波刺激装置の集積化を目指し、微細加工技術を用いて記録用電極とマイクロサイズのトランスデューサ（ダイアフラム）を併設したデバイスを開発した。当初の数値目標を達成し、神経活動を誘起できるマイクロトランスデューサとその活動を記録できる電極を有するデバイスの製作が可能になった。今後は、さらに集積化を押し進め、トランスデューサのダイアフラムを200個程度備えた多配列刺激装置を開発し、頭部を覆う小型ウェアラブルデバイスに応用する予定である。また、超音波の神経活動誘発機序の解明に応用するため、脳切片の単一細胞の電気的活動計測に利用が可能な実験装置へと本研究課題で開発したデバイスを展開する予定である。

本助成金による主な発表論文、著書名

［口頭発表］

1） Ryo Furukawa, Hiroki Kaneta, and Takashi Tateno, “A spatiotemporal analysis of ultrasound-driven responses reflecting acoustic pressure distributions and cortical circuits in mouse brain slices in vitro”（「音響圧分布とin vitroマウス脳スライスの皮質回路網を反映した超音波誘発応答の時空間的解析」）, 第45回日本神経科学大会（NEURO2022）, 2022年7月2日. 3P-313, 開催地：沖縄.

2） Ryo Furukawa and Takashi Tateno, A piezoelectric micromachined ultrasound transducer with the interface of simultaneous measurement of neural activity in vitro, SS2-1, 2022年 電気学会 電子・情報・システム部門大会（2022 Annual Conference of Electronics, Information and Systems, IEE of Japan）, 2022年8月31日～9月3日, 開催地：広島市.